RESEARCH AND OPTIMIZATION OF SPORT UTILITY VEHICLE AERODYNAMIC DESIGN

UDC:533.6.01:629.33
Original scientific paper https://doi.org/10.46793/aeletters.2024.9.2.5

Vu Hai Quan[1*]

[1] School of Mechanical and Automotive Engineering, Ha Noi University of Industry (HaUI), Ha Noi 100000, Vietnam

Abstract:
Drag and lift are two important parameters to evaluate a vehicle's aerodynamic performance. Aerodynamic resistance (drag force F_d) prevents the movement of the vehicle and has a value proportional to the square of the velocity. That is, when the speed increases twice, the aerodynamic drag will increase fourfold. This article presents a plan to design a sport utility vehicle model with improved aerodynamics by using Ansys Fluent software to analyze pressure distribution areas that affect aerodynamics and the body. Based on the results obtained, the areas of stress and maximum pressure concentration have been identified. From this, a plan to improve the vehicle's exterior design has been proposed. After many iterations of the design and model optimization process, the aerodynamic drag coefficient C_D was reduced by 3.06% compared to the original model. The revised design option is equipped with an airflow diffuser under the vehicle; the lifting resistance coefficient has been reduced from 0.0902 to 0.038, equivalent to 58.2%. The new proposed design of the model has reduced the vehicle's frontal drag by 2.04%. The research results have determined the aerodynamic coefficients C_D and C_L of the model car. Based on the results received, it is possible to compare them with the manufacturer's announced parameters and propose new design options that still ensure aesthetics.

ARTICLE HISTORY
Received: 29 March 2024
Revised: 13 June 2024
Accepted: 26 June 2024
Published: 30 June 2024

KEYWORDS
Aerodynamic Drag, Coefficient of Drag, CFD, Concept Car, NX, Ansys Fluent

1. INTRODUCTION

When cars run on the highway at 60-80 km/h, approximately 40-50% of the total energy is required to overcome aerodynamic drag. In urban driving conditions, at average speeds 40 km/h, about 25% of fuel consumption is used to counteract air resistance. Aerodynamic drag significantly impacts the energy efficiency of vehicles. Characterized by the frontal drag coefficient C_D, which is a parameter that depends on the aerodynamic shape of the vehicle body. Advances in automotive technology reveal a trend toward producing faster, more powerful, and lighter vehicles. One of the critical criteria in modern car design is ensuring overall safety, specifically stability and control over the vehicle [1,2]. SUVs face significant challenges with higher air resistance compared to sedan models. This is due to the high rake angle, causing the airflow to separate early at the roof end. This phenomenon leads to increased drag resistance due to a high degree of turbulence behind the vehicle [3,4].

Various studies have also been conducted on the effects of mirrors and rear windshields. In the research [5], the authors performed to simulate the influence of geometric parameters on the aerodynamic drag coefficient C_D. In the research [6] comparison of design options was performed on a large SUV model with the aim of finding the optimal design option. In the research [7] closed and open cooling apertures for SUVs were studied

*CONTACT: Vu Hai Quan, e-mail: quanvh@haui.edu.vn

experimentally to know their effect on drag resistance. The research [8] was carried out for a Fiat Linea car model with a scale of 1/5 size to evaluate the influence of model scale on the pressure distribution area and drag coefficients C_D were performed. The design problem of adding a diffuser to the rear of the car was solved by the authors [9], which resulted in an improvement of the aerodynamic drag coefficient by about 4%. The pressure difference between the front and rear distribution areas is the main factor that creates drag on SUVs, accounting for more than half of the aerodynamic drag value [10]. By optimizing the aerodynamic shape of passenger cars, it is possible to help reduce aerodynamic drag. In the research [11], it was shown that the drag coefficient C_D of the Sonata model was improved after changing the rear shape of the car. The k–ε flow models in aerodynamic research were mentioned in papers [1,12]. In the research [13], the effects of different flow types were analyzed using the SolidWorks Flow tool. The simulation model was performed with many different truck models and SUVs; these vehicle models were having an increasing market share. The purpose of the study was to evaluate the factors affecting the aerodynamic drag coefficient C_D. In the research [14], test measurements of the truck model were carried out in the wind tunnel, the ratio of the experimental model and the actual vehicle was 1/24. In the research [15] it was studied and proposed aerodynamically optimized exterior designs of a sport utility vehicle using computational fluid dynamics analysis based on Reynolds' steady-state average Navier-Stokes turbulence models. In research [16] ANSYS Fluent was used to calculate the vehicle's Drag and Lift Factor. After simulating the conventional flow, an Adjoint solver was used to determine its shape sensitivity in relation to the observed i.e., pulling and lifting. In the research [17], the first experimental one was performed design (DoE) was performed with Large Vortex Simulation (LVS), involving height geometric parameters for the radial base function of the front air dam, using the Sobol algorithm. Then, a multi-objective genetic algorithm (MOGA) was constructed and applied to an alternative model, depending on the geometric parameters of the front windshield. In the research [18], the connection between the possibility of reducing the aerodynamic resistance of the vehicle and the air resistance coefficient was examined. This drag affects the fuel consumption of the vehicle because the vehicle speed is higher. There are actual values evaluated of the vehicle's air resistance coefficient, devices that can reduce air resistance, and the effect of selected aerodynamic devices on reducing drag and reducing fuel consumption. In the research [19] CFD calculations and analyses typically specific to high-performance vehicles were performed and applied to passenger vehicles such as SUVs and sedans. The results show that on average, the resistance coefficient decreases by 16% and the lifting coefficient decreases by 232% on a large scale [19].

2. THEORETICAL FOUNDATIONS OF AUTOMOTIVE AERODYNAMICS RESEARCH

2.1. Overview of Car Aerodynamics

There are 6 types of aerodynamics acting on the car. Aerodynamics influence the car mainly through aerodynamics and aerodynamic torque.

Driving speed, body shape, and vehicle slip angle are important factors affecting aerodynamic forces and aerodynamic torque. Aerodynamic force and moment are composed of 3 axial forces and moments around X and Y axis, and Z axis, also known as 6 aerodynamic component forces, mainly including drag force F_d, lift force F_l, lateral force F_S, rolling moment T_{RM}, lifting torque T_{PM} and yawing moment T_{YM}.

According to ISO standards, the aerodynamic origin is located at the center of the front and rear axles. The six aerodynamic component forces are determined as follows according by equation 1 [20]:

$$\begin{cases} F_D = \frac{1}{2} C_D A_\rho u^2 \quad F_L = \frac{1}{2} C_L A_\rho u^2 \quad F_S = \frac{1}{2} C_S A_\rho u^2 \\ T_{RM} = \frac{1}{2} C_{RM} A_\rho L u^2 \quad T_{RM} = \frac{1}{2} C_{RM} A_\rho L u^2 \\ T_{YM} = \frac{1}{2} C_{YM} A_\rho L u^2 \end{cases} \quad (1)$$

where are: F_D is drag force (N), F_L is lifted (N), F_S is lateral force (N), C_L is lift coefficient, C_D is drag coefficient, C_S is lateral force factor, T_{RM} is moment rolling (Nm), T_{PM} is the thrust torque (Nm), T_{YM} is the rotational torque (Nm), C_{RM} is the torque coefficient in the X direction, C_{PM} is the torque coefficient in the Y direction, C_{YM} is the torque coefficient in the Z direction, A is the projected area of the car (m^2), ρ is the air density (kg/m^3), L is the wheelbase (m), and u is the velocity (m/s).

2.2. Flow Model in Research

The k-epsilon model is the simplest turbulent flow model in its complete form with two

descriptive equations that are independently solved based on the transformation equation of turbulence velocity and turbulence length ratio. The computational model has the characteristics of being simple, saving time, and having moderate accuracy, but because of the calculation for the turbulence of the flow over a wide range (Reynolds variation is large), this model is widely used in industrial calculations. This is a semi-empirical computational model derived from theoretical equations combined with an experiment based on the researcher's experience. Analyzing the strengths and weaknesses of the computational model, the simulation model has been chosen for research.

This model applies independent solving of two transformation equations: entanglement kinetic energy (k) and diffusion rate (ε) [21]:

$$\begin{cases} \frac{\partial}{\partial_t}(\rho k)+\frac{\partial}{\partial_{x_i}}(\rho k u_i)=\frac{\partial}{\partial_{x_j}}\left[\left(\mu+\frac{\mu_t}{\sigma_k}\right)\frac{\partial k}{\partial_{x_j}}\right]+G_k+G_b-\rho\varepsilon-Y_M+S_k \\ \frac{\partial}{\partial_t}(\rho\varepsilon)+\frac{\partial}{\partial_{x_i}}(\rho\varepsilon u_i)=\frac{\partial}{\partial_{x_j}}\left[\left(\mu+\frac{\mu_t}{\sigma_k}\right)\frac{\partial\varepsilon}{\partial_{x_j}}\right]+C_{1\varepsilon}\frac{\varepsilon}{k}(G_k+C_{3\varepsilon}G_b)-C_{2\varepsilon}\rho\frac{\varepsilon^2}{k}+S_\varepsilon \end{cases} \quad (2)$$

where are:

μ_t- Turbulent viscosity (kg/m·s);

μ:- dynamic viscosity (kg/m·s);

u_i - velocity component (m/s);

G_k - Represents the generation of entangled kinetic energy due to the average velocity gradient (kg/m·s³);

G_b - Kinetic energy generation due to buoyancy (kg/m·s³);

Y_M - Shows variable expansion in compressible turbulent flow (kg/m·s³);

$C_{1\varepsilon}$, $C_{2\varepsilon}$ - Constants ($C_{1\varepsilon}$ = 1.44; $C_{2\varepsilon}$ = 1.92);

$C_{3\varepsilon}$: Shows e's exposure to buoyancy;

S_k, S_ε - The entanglement coefficients of k and e (S_k = 1; S_ε = 1,3);

S_k, S_ε - User-defined function that depends on the problem condition.

2.3. Methodology and Methods

In this research, Ansys Version R19.2 software and NX model design software were used to build and access calculations installed at the School of Mechanical and Automotive Engineering, Hanoi University of Industry. Model design parameters are based on specific objects, and are proposed to be adjusted with different options to run tests and obtain results. The methodology used is shown in Fig. 1.

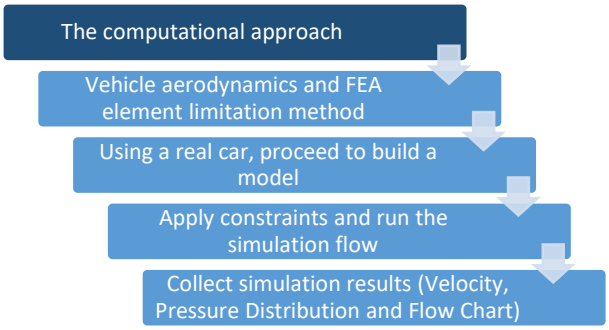

Fig. 1. Procedure for analyzing aerodynamic problems

In the computational approach, the model designed by NX is used for rendering purposes to make the model realistic, Ansys Fluid Flow Simulation is then applied for simulation purposes. Various result viewing options related to Flow Simulation are applied to analyze the models. Options for viewing results.

- Shear diagram (Shows pressure distribution, velocity distribution, etc.)
- Surface diagram (Shows pressure distribution.)
- Flow trajectory.

Simulation results of velocity, pressure distribution, flow trajectory, mesh diagrams, parameters of displacement of drag coefficients, and distribution of drag force acting on the vehicle need to be presented visually.

The simulation process is performed sequentially with four proposed design options with the same boundary conditions. The simulation results have determined the frontal resistance coefficient C_D and the lift resistance coefficient C_l:

1. Original car model with 55° front windshield angle.
2. Improved car model with 60° front windshield angle.
3. Improved car model with 65° front windshield angle.
4. Improved vehicle model with air diffuser.

2.4. Analysis of the components of aerodynamic resistance acting on the vehicle

(a) The resistance force that a flowing fluid exerts on an object in the direction of flow is called drag. Resistance is due to the combined effect of pressure and wall shear in the direction of flow. The equation determines the tensile force due to the combined effect of the wall shear stress and the compressive force [22]:

$$F_d = \frac{1}{2}\rho V^2 C_D A \quad (3)$$

where are: F_d - Frontal resistance (N); ρ - air density (kg/m^3); V - relative speed (m/s); C_D - coefficient of frontal drag; A - area of the front bumper (m^2).

Aerodynamic drag consists of two main components: frictional resistance and pressure resistance. Pressure drag accounts for more than 80% of total drag, and the condition is highly dependent on the geometry of the vehicle due to the separation of the boundary layer from the rear window surface and the formation of a wake-up zone behind the vehicle.

(b) Lifting air is similar to drag but also creates an opposing force to drag. It is created when air flows over a curved surface. The gas pressure in the gas stream decreases, and outside forms a lift on that surface, causing an uplift.

The equation for lifting air resistance of the vehicle can be presented [23]:

$$F_L = \frac{1}{2}\rho V^2 C_L A \quad (4)$$

where are: F_L - Lifting force (N); ρ - air density (kg/m^3), V - relative speed (m/s), C_L - system upgrade and A - raised area (m^2).

(c) Streamline: A streamline is an imaginary line drawn in the flow field such that a tangent drawn at any point on the line represents the direction of the velocity vector.

(d) Vorticity: Vorticity is a measurement of the rotation of a fluid particle. More specifically, Vorticity is equal to twice the angular velocity of the liquid particle. For racing cars and other high-speed aerodynamic vehicles, vortex forces have a greater effect. The vortex force creates flow leakage. From the high-pressure side to the low-pressure side.

(e) Computational Fluid Dynamics (CFD) is a powerful tool in the field of fluid mechanics. It is one of its branches that uses numerical methods and algorithms to solve and analyze problems related to fluid flow. By providing numerical solutions to the governing equations of fluid dynamics throughout the desired flow region, CFD allows for the solution of complex problems without oversimplification. This dynamic capability of CFD is a significant advancement in the field of fluid mechanics, and understanding its principles is crucial for any professional or academic in this field.

3. DESIGN AND SIMULATION

3.1 Drawing and Designing The Car Models in Software

In this research, a reference model of a sports utility vehicle (SUV) was used. Dimensions of the vehicle are shown in Fig. 2. The width is 1981 mm, the height is 1910 mm, the wheelbase length is 2849 mm, and the overall length is 5064 mm.

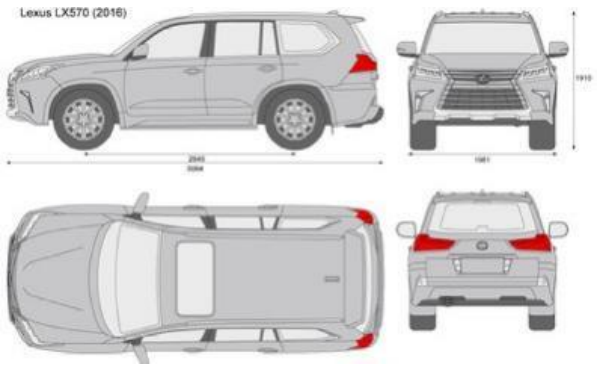

Fig. 2. Schematic representation of the vehicle (Linear distance in millimetres and angle in degrees)

The vehicle shape is referenced based on the Lexus LX570. Through the actual available dimensions, an SUV model was constructed for evaluation. The design model proposed in the research includes some assumptions that have not been considered, such as the influence of rearview mirrors, tyres, and door handles on the vehicle's aerodynamic properties, Fig. 3.

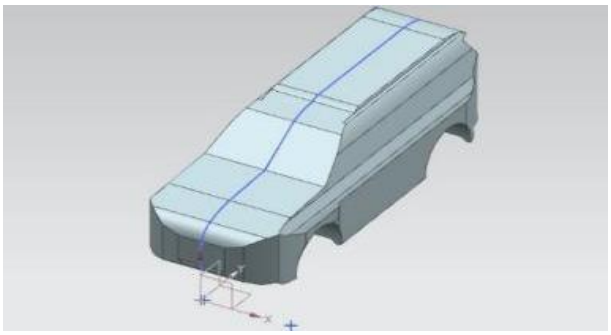

Fig. 3. Three-dimensional solid model of the model vehicle in the NX application

3.2 Aerodynamic Analysis of the Original Model

The results in Fig. 4 show the velocity distribution inside the simulation area of the aerodynamic tube, mesh and isolation lines to delineate the internal velocity distribution. The results are observed in the results bar to the left of the graph with the original car model with front windshield angle 55^o.

Fig. 4 shows the velocity distribution around the model. The red region represents the high-velocity region, the blue region represents the low-velocity region, and the dark blue region represents zero velocity.

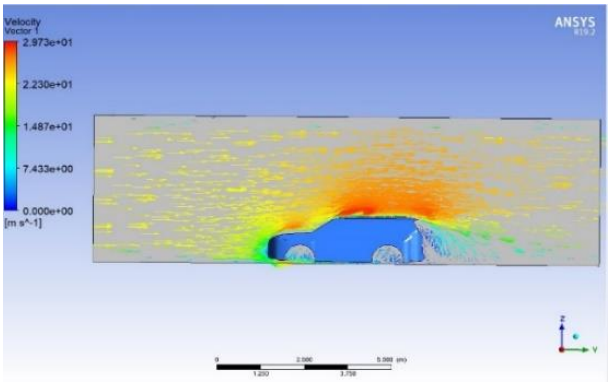

Fig. 4. Velocity distribution of elements around the vehicle model at an angle of 55°

The results show that low air velocity is distributed in the front and rear areas of the vehicle. The speed tends to increase, with the top part of the car's roof reaching the highest speed value. The airflow velocity over the hood decreases significantly and remains constant as the airflow flows toward the rear of the vehicle in the direction of airflow displacement. In the front area, there are some areas where the airflow is blocked, so the velocity of air particles here is lower than on the roof.

The simulation results in Fig. 5 show the pressure distribution shown in the aerodynamic duct simulation area inside the contours. The light blue area represents low pressure, and the red area is high pressure. The area in front of the vehicle has a greater pressure concentration than other areas because the velocity is small here. In fact, car manufacturers are always looking for ways to improve the design of the vehicle's front area to reduce the value of this high-pressure distribution area.

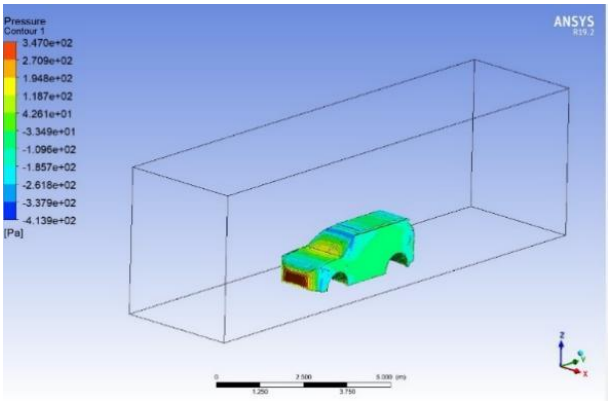

Fig. 5. Pressure distribution of the car model at an angle of 55°

According to the theoretical basis of the Bernoulli effect, when the difference in pressure distribution area in front and rear of the vehicle is too large, it causes 80% of the frontal resistance value. Therefore, when the vehicle moves, it will have to consume significant energy to overcome this resistance. Therefore, the front and rear areas of the vehicle will be the target locations for proposing appropriate aerodynamic design options.

The results in Fig. 6 showing the flow trajectory show that the flow of the flow is not organized with respect to the shape of the model but needs to be smooth to maintain a continuous uniform flow. If the air flow passes completely without obstacles, the velocity of the model will increase. Therefore, areas where gas flows encounter obstacles need to be modified. Specifically, the sharp edges of the vehicle should be modified to control smooth flow.

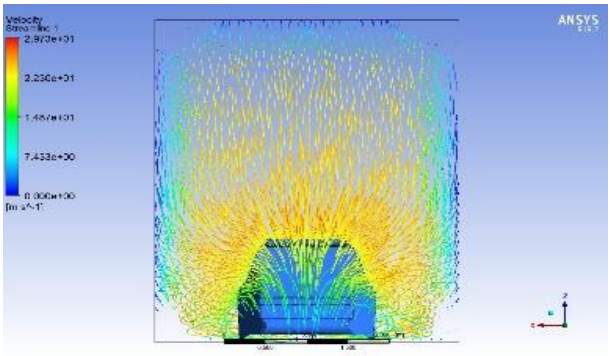

Fig. 6. The flow trajectory of the vehicle model at an angle of 55°

3.3 Target Areas for Modification

From the analysis of the vehicle's aerodynamics, the survey results discovered certain areas where high-pressure areas are concentrated, and vortex flows are formed in Fig. 7. Therefore, these are the areas that were chosen as the target to modify the vehicle's appearance. These locations are marked to consider changing the slope angle and size of the vehicle in order to optimize the vehicle's shape and aerodynamics, thereby adjusting the frontal resistance and lifting resistance values of the car.

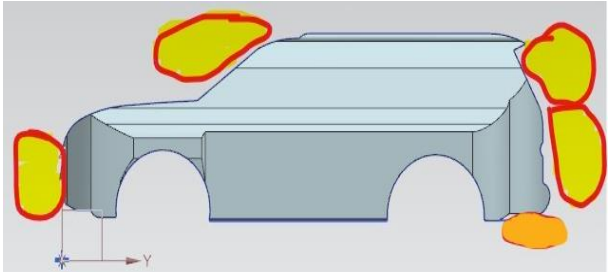

Fig. 7. Modification locations

3.4. Modified Car Model Design

Based on the simulation results in sections 3.2 and 3.3, after determining the areas and locations that need to be modified, the vehicle's simulation model will be adjusted to improve the air resistance coefficient. The vehicle's kinetic energy is C_D and C_L.

The calibration of the model is guided by a set of globally recognized standards for windshield placement angles. These standards, which are not confined to a specific region, are designed to ensure the safety of the driver and passengers during vehicle operation. They also play a crucial role in maintaining vehicle anthropometric and aerodynamic standards. Some of the reference standards include:

1. American FMVSS standard: (Federal Motor Vehicle Safety Standards) standard stipulates a minimum windshield angle of 70° and a minimum front window glass angle of 25° [24].

2. The European ECE standard (Economic Commission for Europe) stipulates a minimum windshield angle of 75° and a minimum front window glass angle of 65° [25].

3. The Japanese JIS standard: (Japanese Industrial Standard) standard stipulates a minimum windshield angle of 70° and a minimum front window glass angle of 25° [26].

The establishment of these standards is not a mere formality, but a crucial step in ensuring the safety of the driver and passengers. They provide a wide and sufficient field of view, aiding the driver in assessing the surrounding space of the vehicle. It is imperative for car manufacturers to adhere to these standards during the vehicle design process. This is not only to ensure safety but also to comply with legal regulations before the vehicle is put into circulation on the road.

For the front windshield area, increasing the windshield angle and decreasing the sunlight angle will reduce the visibility distance. Therefore, the worst visibility distance is obtained when the windshield tilt angle is 70°, and the sunlight angle is 10°. The windshield angle that achieves the farthest viewing distance is 55° with a sunlight angle of 30 degrees, giving a viewing distance of approximately 800 m. For an angle of 60° and a sunlight angle of 30°, the viewing distance will be approximately 650 m. With an angle of 65° and a sunlight angle of 30°, the viewing distance will be approximately 670 m [27]. Therefore, the calibrated design plan will select the vehicle's front windshield angle with three parameter cases: 55°, 60° and 66°.

The vehicle's underbody is equipped with a diffuser to reduce its lift force. The drawing and dimensions are shown in Fig. 8.

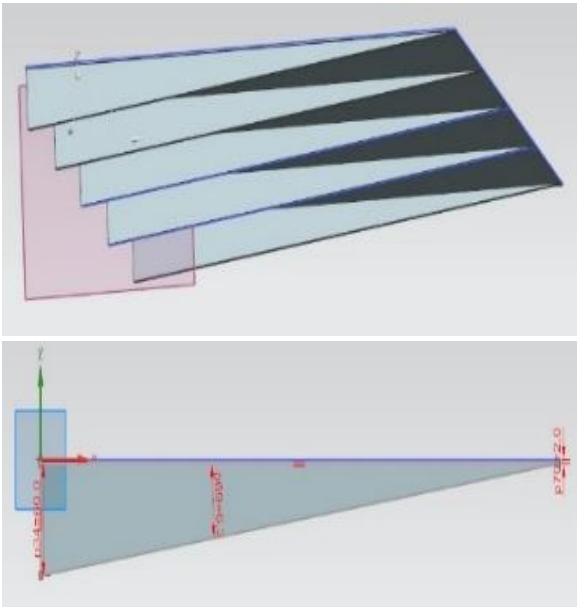

Fig. 8. Airflow diffuser model and Dimensions of diffuser

The proposed design option to improve car aerodynamics after adjustment is shown in Fig. 9, 10 and 11.

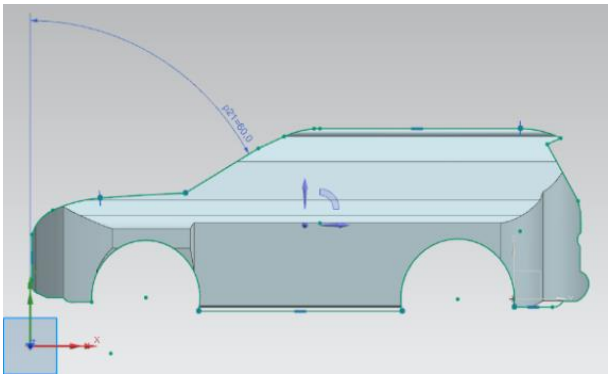

Fig. 9. Modified car model with 60° front windshield angle

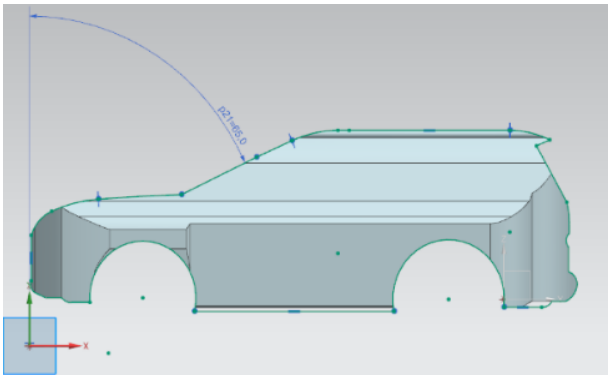

Fig. 10. Modified car model with front windshield angle 65°

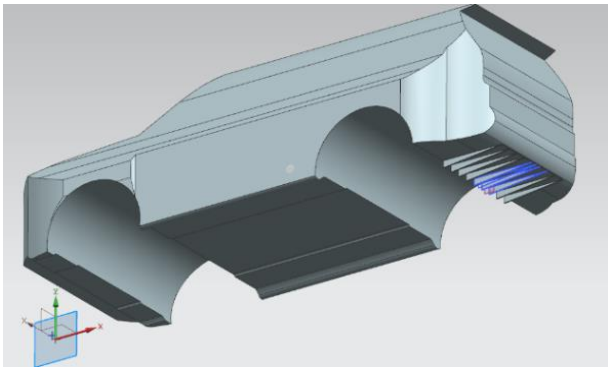

Fig. 11. Modified vehicle model with air flow diffuser

4. EVALUATION OF THE PROPOSED DESIGN

4.1 Target Areas for Modification

4.1.1 Modified Car Model with a 60° Front Windshield Angle

The simulation results in Fig. 12 show that the velocity distribution on the simulation model changed when the spectrum of the velocity region in front of the windshield decreased from dark yellow to lighter yellow. That means the airflow velocity decreases from about 22.3 - 29.7 m/s to 15.9 - 23.97 m/s. Similarly, in the area above the car's roof, the air velocity also tends to decrease. Simulation results show that design adjustments will affect the flow distribution and pressure partition. Therefore, in design, consideration should be given to adjusting appropriate values based on standards.

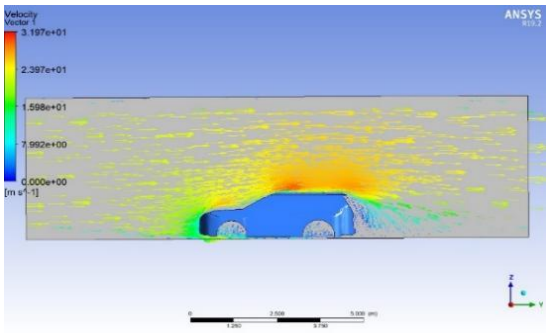

Fig. 12. Velocity distribution of the surrounding airflow of the vehicle at an angle of 60°

The simulation results shown in Fig. 13 show that the pressure distribution on the model has been modified by using aerodynamic properties to reduce the front windshield, helping to reduce the concentrated pressure distribution area. Comparison to the stock model shows that the use of these aerodynamic edges and revised shape treatment reduces the impact of pressure on the revised vehicle profile. The colour diagram (Magnitude of stress acting on positions on the vehicle's face) clearly shows the pressure effect on the surface of the object.

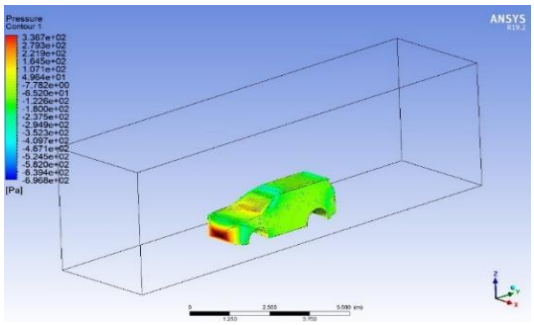

Fig. 13. Model of pressure distribution of the vehicle at an angle of 60°

Fig. 14 shows the flow trajectory results representing the modified vehicle velocity. The results show that the air on the moving path of the model after improvement is less hindered than in the original model. The velocity of the flow on the vehicle tank, which shows the yellow area, is 23.97 m/s. On the hood, the model shows red lines where the velocity increases and the velocity is 31.97 m/s. On the back side, there is a green area with a velocity value of 15.98 m/s.

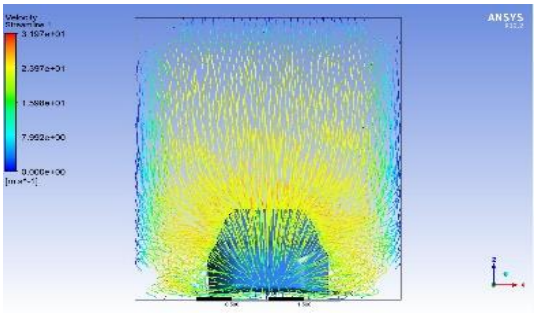

Fig.14. Airflow trajectory of the vehicle model at an angle of 60°

4.1.2 Modified Car Model with a 65° Front Windshield Angle

Analyzing the wind speed distribution results of the modified model in Fig. 15 shows that the maximum wind speed has decreased but the total speed on the car's roof has increased. The frontal windshield corner resistance area has improved flow speed. Air resistance is reduced from about 15.9 - 23.97 m/s for 60°, then for 65° to 15.29 - 22.94 m/s which has improved slightly.

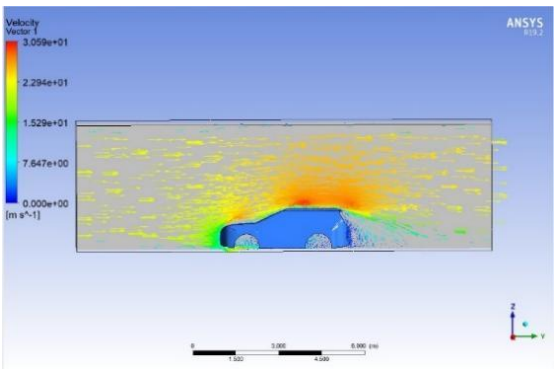

Fig. 15. Velocity distribution of the vehicle's surrounding air at an angle of 65°

4.2 Comparison and Comments on the Aerodynamic Improvements of the Car

The simulation process is performed sequentially with four proposed design options with the same boundary conditions. The simulation results have determined the frontal resistance coefficient C_D and the lift resistance coefficient C_L. These parameters are listed in Table 1.

Table 1. Statistics of coefficients C_D and C_L in each case

coefficient	55°	60°	65°	Attach the airflow diffuser
C_D	0.5925	0.5824	0.5744	0.5896
C_L	0.0902	0.0995	0.0972	0.0377

Statistical results from Table 1 and Figs. 16 and 17 show that when the front windshield angle increases from 55° to 65°, the C_D coefficient decreases from 0.5925 to 0.577. However, the C_L coefficient is not much affected by this adjustment. In Fig. 17, the C_L coefficient decreases from 0.0902 to 0.0377 when the original design model is equipped with an airflow diffuser under the vehicle.

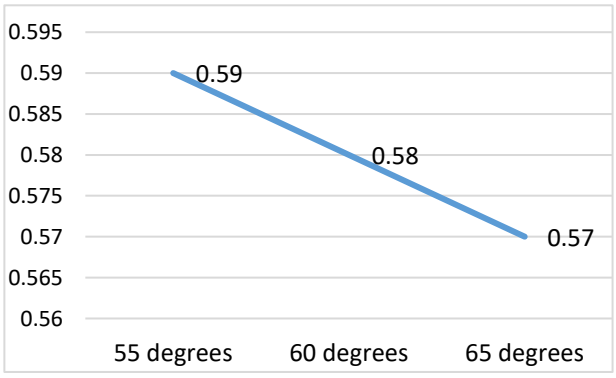

Fig 16. C_D coefficient

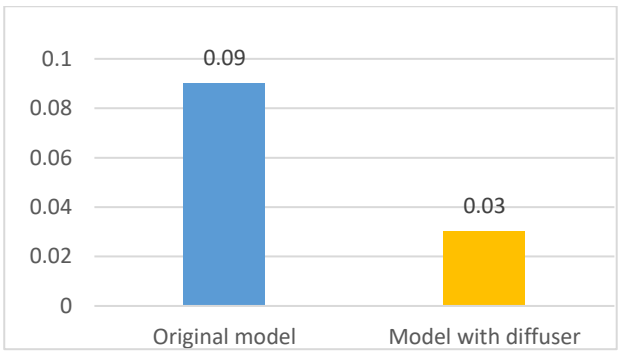

Fig 17. C_L coefficient

The results in Fig. 18 show the frontal aerodynamic resistance of the three front glass corners with the same vehicle speed condition of 100 km/h. Frontal drag has been reduced from 561.36 N to 549.87 N.

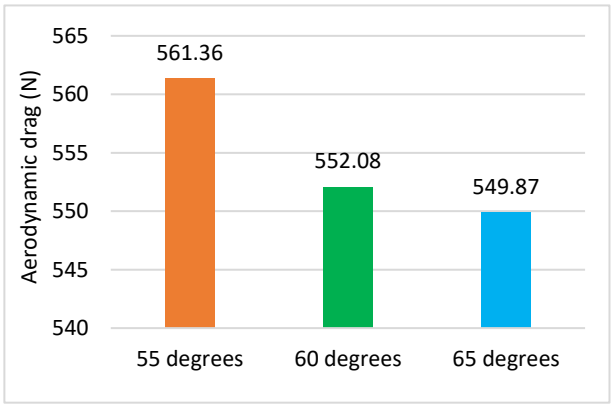

Fig 18. Frontal drag in 3 cases at 100 km/h

The results in Fig. 19 show the change in lift force when equipped with an air diffuser under the rear of the car from 54.788 N down to 23.089 N. It can be seen that the shape of the vehicle greatly affects the vehicle's aerodynamic drag. Through changes at the front of the vehicle, such as reducing the frontal contact area of the vehicle, better directing the airflow and reducing the area of the rear vortex. For the front glass, the tilt angle can be reduced to reduce gas concentration at the points from the hood to the vehicle's windshield, causing obstructions to the vehicle. For the rear glass, the tilt angle can be increased to reduce the difference in vacuum pressure. The large pressure difference is one of the main factors causing the Bernoulli principle phenomenon to create vacuum regions. The larger the area the vacuum pressure area will create greater resistance, causing the vehicle speed to be greatly reduced at high-speed ranges, causing unnecessary fuel wastage. Evaluation results are shown in statistical Table 1 and Fig. 19.

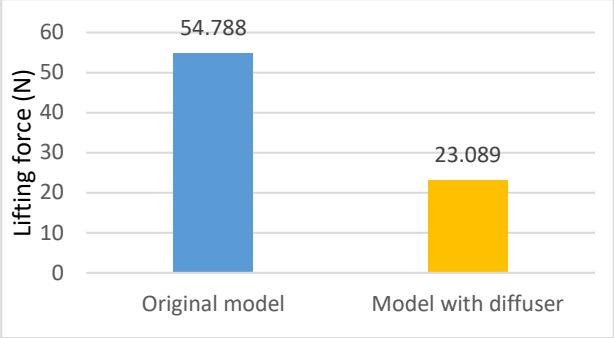

Fig 19. Two fields of Lifting force of the vehicle in the case

Regarding the lift coefficient, an additional diffuser under the vehicle is proposed to direct air flows and minimize the formation of turbulent air flows. Less turbulence of the airflow at the rear and underbody of the vehicle reduces the effect of the Bernoulli principle, as demonstrated through simulation results.

4. CONCLUSION

The main objective of this research is to design a Sport utility vehicle model with improved aerodynamics by using Ansys Fluent software to analyze stress zones affecting aerodynamics and improve the shape. car model shape. After many iterations of model design and optimization, the aerodynamic drag coefficient C_D has been reduced by 3.0548% compared to the original model. For the revised design and the addition of an air-flow diffuser under the vehicle, the lift coefficient has been reduced from 0.0902 to 0.0377, reducing the lift coefficient by 58.2%. The new design of the new model has reduced the vehicle's frontal drag by 2.04%.

This research has found the aerodynamic coefficients C_D and C_L of the model SUV. However, many shortcomings still need to be further improved on the surface of speed, airflow, and pressure distribution around the vehicle to reduce the aerodynamic coefficient. The research focused on using the vehicle model going through the tube when the characteristic kinematics are simulated by the software. The results of the research have determined the drag coefficient and proposed an aerodynamic design that allows for improved C_D and C_L coefficients compared to the original design.

Aerodynamics research is a complex problem, requiring in-depth research on flow in different states. In the next studies, the authors will develop different flow models, combining simulation research with experimental research.

Conflicts of Interest

The author declares no conflict of interest.

REFERENCES

[1] R.C. Das, M. Riyad, CFD analysis of passenger vehicle at various angle of rear end spoiler. *Procedia engineering*, 194, 2017: 160-165. https://doi.org/10.1016/j.proeng.2017.08.130

[2] S. Srinivasarao, V. Lakshamaih, CFD Research on Car Body. *International Journal of Recent Technology and Engineering (IJRTE)*, 8(2S3), 2019: 1178-1180. https://doi.org/10.35940/ijrte.B1218.0782S319

[3] R. Tarakka, N. Salam, Jalaluddin, W. Rauf, M. Ihsan, Aerodynamic drag reduction on the application of suction flow control on vehicle model with varied upstream velocity. *IOP Conference Series: Materials Science and Engineering*, 1173, 2021: 012045. https://doi.org/10.1088/1757-899X/1173/1/01204

[4] L. Sterken, S. Sebben, L. Löfdahl, Numerical implementation of detached-eddy simulation on a passenger vehicle and some experimental correlation. *Journal of Fluids Engineering*, 138(9), 2016: 091105. https://doi.org/10.1115/1.4033296

[5] V. Sirenko, R. Pavlovs'ky, U.S. Rohatgi, Methods of reducing vehicle aerodynamic drag. *Proceedings of the ASME 2012 Fluids Engineering Division Summer Meeting collocated with the ASME 2012 Heat Transfer Summer Conference and the ASME 2012 10th International Conference on Nanochannels, Microchannels, and Minichannels*, Vol.1, USA, 8-12 July 2012, Rio Grande, Puerto Rico, pp.97-102. https://doi.org/10.1115/FEDSM2012-72491

[6] Y.A. Brown, S. Windsor, A.P. Gaylard, The effect of base bleed and rear cavities on the drag of an SUV. *SAE Technical Paper*, 2010: 2010-01-0512. https://doi.org/10.4271/2010-01-0512

[7] J. Pitman, A. Gaylard, An experimental investigation into the flow mechanisms around an SUV in open and closed cooling air conditions. *Progress in Vehicle Aerodynamics and Thermal Management. FKFS 2017. Springer, Cham,* 2018: 61-79. https://doi.org/10.1007/978-3-319-67822-1_4

[8] A. Altinisik, E. Kutukceken, H. Umur, Experimental and numerical aerodynamic

analysis of a passenger car: Influence of the blockage ratio on drag coefficient. *Journal of Fluids Engineering*, 137(8), 2015: 081104. https://doi.org/10.1115/1.4030183

[9] S.-O. Kang, S.-O. Jun, H.-I. Park, K.S. Song, J.D. Kee, K.H. Kim, D.H. Lee, Actively translating a rear diffuser device for the aerodynamic drag reduction of a passenger car. *International Journal of Automotive Technology*, 13, 2012: 583-592. https://doi.org/10.1007/s12239-012-0056-x

[10] A. Wood, M. Passmore, D. Forbes, D. Wood, A. Gaylard, Base pressure and flow-field measurements on a generic SUV model. *SAE International Journal of Passenger Cars-Mechanical Systems*, 8(1), 2015: 233-241. https://doi.org/10.4271/2015-01-1546

[11] K.S. Song, S.O. Kang, S.O. Jun, H.I. Park, J.D. Kee, K.H. Kim, D.H. Lee, Aerodynamic design optimization of rear body shapes of a sedan for drag reduction. *International Journal of Automotive Technology*, 13, 2012: 905-914. https://doi.org/10.1007/s12239-012-0091-7

[12] H. Harinaldi, B. Budiarso, W. Warjito, E.A. Kosasih, R. Tarakka, S.P. Simanungkalit, L. Teryanto, I.G.M. Fredy, Modification of flow structure over a van model by suction flow control to reduce aerodynamics drag. *Makara Journal of Technology*, 16(1), 2012: 3. https://doi.org/10.7454/mst.v16i1.1021

[13] W. Kim, J. Noh, J. Lee, Effects of vehicle type and inter-vehicle distance on aerodynamic characteristics during vehicle platooning. *Applied Sciences*, 11(9), 2021: 4096. https://doi.org/10.3390/app11094096

[14] T. Skrucany, B. Sarkan, J. Gnap, Influence of aerodynamic trailer devices on drag reduction measured in a wind tunnel. *Eksploatacja i Niezawodnosc – Maintenance and Reliability*, 18(1), 2016: 151-154. http://dx.doi.org/10.17531/ein.2016.1.20

[15] A. Al-Saadi, K. Al-Farhany, K.K.I. Al-Chlaihawi, W. Jamshed, M.R. Eid, E.S.M. Tag El Din, Z. Raizah, Improvement of the aerodynamic behavior of a sport utility vehicle numerically by using some modifications and aerodynamic devices. *Scientific Reports*, 12, 2022: 20272. https://doi.org/10.1038/s41598-022-24328-w

[16] A. Rehmat, Fayyaz, S. Bashmal, M. Sharif, S. Khan, Numerical modeling of the shape optimization for a commercial car by decreasing drag and increasing stability. *Arabian Journal for Science and Engineering*, 48, 2023: 12427-12437. https://doi.org/10.1007/s13369-023-07834-5

[17] C. Erdem, Y. Eulalie, P. Gilotte, S. Harries, C.N. Nayeri, Aerodynamic Optimization of a Reduced Scale Model of a Ground Vehicle with a Shape Morphing Technique. *Fluids*, 7(5), 2022: 166. https://doi.org/10.3390/fluids7050166

[18] T. Skrucany, S. Semanova, S. Milojević, A. Ašonja, New technologies improving aerodynamic properties of freight vehicles. *Applied Engineering Letters*, 4(2), 2019: 48-54. https://doi.org/10.18485/aeletters.2019.4.2.2

[19] S. Piratla, Evaluating the aerodynamics of different passenger vehicle configurations. *TechRxiv*, 21, 2023. https://doi.org/10.36227/techrxiv.24139254.v1

[20] J. Wang, H. Li, Y. Liu, T. Liu, H. Gao, Aerodynamic research of a racing car based on wind tunnel test and computational fluid dynamics. *MATEC Web of Conferences*, 153, 2018: 04011. https://doi.org/10.1051/matecconf/201815304011

[21] A. Dewan, k–ε and Other Two Equations Models. *In: Tackling Turbulent Flows in Engineering. Springer Berlin Heidelberg*, 2011: 59-79. https://doi.org/10.1007/978-3-642-14767-8_6

[22] Y. Gan. L. Li, Optimization of Aerodynamic Profile of Ground Vehicle. *Journal of Physics: Conference Series*, 2569, 2023: 012068. http://dx.doi.org/10.1088/1742-6596/2569/1/012068

[23] P.A. Tuan, V.D. Quang, Estimation of car air resistance by CFD method. *Vietnam Journal of Mechanics*, 36(3), 2014: 235-244. https://doi.org/10.15625/0866-7136/36/3/4176

[24] CD and CAFE Standards. *National Highway Traffic Safety Administration (NHTSA)*. https://www.nhtsa.gov/sites/nhtsa.gov/files/2023-07/CAFE-2027-2032-HDPUV-2030-2035-NPRM-web-version.pdf (Accessed: 15 March 2024).

[25] Euro Standard. *European European Union standardisation*. https://eur-lex.europa.eu/EN/legal-content/summary/european-union-standardisation.html (Accessed: 15 March 2024).

[26] JIS Standards. *Japanese Industrial Standards - JIS.* https://www.jisc.go.jp/index.html (Accessed: 15 March 2024).

[27] V.D. Bhise, S. Sethumadhavan, Predicting Effects of Veiling Glare Caused by Instrument Panel Reflections in the Windshields. *SAE International Journal of Passenger Cars-Electronic and Electrical Systems*, 1(1), 2009: 275-281. https://doi.org/10.4271/2008-01-0666